

## Role of egg white protein gelling capacity on the processability and properties of compression-moulded films

Víctor Baquero-Aznar<sup>a,b</sup>, María L. Salvador<sup>b</sup>, Ángel Fernández-Cuello<sup>c</sup>, Isabel Clavería<sup>c</sup>, Jaime González-Buesa<sup>a,b,\*</sup> 

<sup>a</sup> Departamento de Ciencia Vegetal, Centro de Investigación y Tecnología Agroalimentaria de Aragón (CITA), Instituto Agroalimentario de Aragón - IA2 (CITA-Universidad de Zaragoza), Av. Montañana 930, 50059 Zaragoza, Spain

<sup>b</sup> Grupo de Investigación en Alimentos de Origen Vegetal, Universidad de Zaragoza, Instituto Agroalimentario de Aragón-IA2-(Universidad de Zaragoza-CITA), Miguel Servet 177, 50013 Zaragoza, Spain

<sup>c</sup> Department of Mechanical Engineering, University of Zaragoza, Zaragoza 50018, Spain

### ARTICLE INFO

#### Keywords:

Edible film  
Molecular structure  
Food packaging  
Egg white protein  
Glycerol  
Compression moulding  
Barrier properties

### ABSTRACT

This study aimed to assess the impact of the gelling capacity of powdered egg white protein (EWP) on the processability and properties of compressed-moulded films. Three commercial grades of EWP with varying gelling capacities and three protein-to-plasticiser ratios were selected for film preparation. The EWP structure was characterised by FTIR and XRD, and the relative abundance of proteins was estimated using LC-ESI-MS/MS. The rheological properties of the film-forming solutions (FFS), along with the mechanical, barrier, and optical properties of resulting films, were also evaluated. The EWP samples exhibited differences in secondary structure, soluble protein content, and protein profile, which were reflected in the viscosity, consistency, and elastic modulus of the FFS, all of which increased with gelling capacity. The processability and stability of the FFS were found to depend on the appropriate combination of gel strength and protein-to-plasticiser ratio. In addition to the protein-to-plasticiser ratio, the  $\beta$ -turn abundance in the secondary structure of the EWP film was the parameter most strongly correlated with Young's modulus ( $p < 0.01$ ). However, the barrier properties of the films were significantly influenced solely by the protein-to-plasticiser ratio ( $p < 0.01$ ), with higher plasticiser content resulting in increased oxygen and water vapour permeability.

### 1. Introduction

The packaging industry represents the major application field of plastic materials, and most of the plastics (80.4 %) are obtained from fossil-based materials (Plastics Europe, 2023). Edible films made from natural biopolymers, such as polysaccharides and proteins, have emerged as a promising alternative to plastic packaging due to their renewability, biodegradability, biocompatibility, and non-toxicity (Ghasemlou et al., 2024; Sun et al., 2023; Wu et al., 2023). Among these sources, proteins have gained attention due to their relative abundance and film-formation capacity (Bhaskar et al., 2023; Calva-Estrada et al., 2019). Proteins have a great capacity to interact and form bonds due to the amino acid structure, resulting in films with good mechanical properties and excellent gas barrier properties. However, their predominantly hydrophilic character leads to films with high

sensitivity to moisture and poor water barrier characteristics (Hernández-Izquierdo and Krochta, 2008; Wu et al., 2024).

Egg white protein (EWP) is a widely available, low cost, nutritionally rich, of easy digestion, extensively used in agro-food sector due to its excellent functional properties, including gelling, foaming, and emulsifying abilities (Deng et al., 2022; Ma et al., 2019). As a high-quality protein, EWP primarily consists of ovalbumin (OVA), ovotransferrin, ovomucoid, ovomucin, and lysozyme, some of which exhibit natural antimicrobial properties (Deng et al., 2022; Li et al., 2020). Among these, OVA is the dominant protein, containing free thiol (SH) groups, while other major proteins feature multiple disulfide (SS) bonds, both of which play a crucial role in film formation by enabling strong intermolecular and intramolecular interactions. Additionally, hydrophobic and electrostatic forces contribute to the film's structural integrity, flexibility, and biocompatibility (Dong and Zhang, 2020; Huang et al.,

\* Corresponding author: Departamento de Ciencia Vegetal, Centro de Investigación y Tecnología Agroalimentaria de Aragón (CITA), Instituto Agroalimentario de Aragón - IA2 (CITA-Universidad de Zaragoza), Av. Montañana 930, 50059 Zaragoza, Spain.

E-mail address: [jgonzalez@cita-aragon.es](mailto:jgonzalez@cita-aragon.es) (J. González-Buesa).

<https://doi.org/10.1016/j.fufo.2025.100616>

Received 16 January 2025; Received in revised form 20 March 2025; Accepted 25 March 2025

Available online 26 March 2025

2666-8335/© 2025 The Author(s). Published by Elsevier B.V. This is an open access article under the CC BY-NC-ND license (<http://creativecommons.org/licenses/by-nc-nd/4.0/>).

2020; Qin et al., 2024). EWP easily forms a thin film through alkali and heat treatment (Dong and Zhang, 2020). Due to its excellent processability, EWP film can be produced through extrusion and calendaring processes, resulting in material with a superior resistance to breakage and heat, and less oxygen permeability than commercial polylactic acid-based films while maintaining similar sensitivity to relative humidity, transparency and colour properties (Mihalca et al., 2021; Pranata et al., 2019). Peng et al. (2017) proved that EWP-based films were much more transparent than the other protein films, e.g., soybean protein isolate film, whey protein film and pea protein isolate film (Rojas-Lema et al., 2023; Xiao et al., 2023).

However, the poor tensile strength, high water vapour permeability, water sensibility, and susceptibility to microbial contamination of the EWP films limit their applications (Razi et al., 2023). To overcome these drawbacks, researchers have explored various strategies (Wang et al., 2025), including blending EWP with other proteins (Dong et al., 2022; Jiang et al., 2024; Zhao et al., 2020), developing EWP composites with polysaccharides (Han et al., 2020; Huang et al., 2020; Li et al., 2024; Liu et al., 2022; Qin et al., 2024), mixing with hydrophobic additives as fatty acids, lipids or waxes (Niegelhell et al., 2017), or constructing multi-layer structures with EWP and shellac (Baquero et al., 2024). Some of these films have demonstrated potential for packaging oil, cherry tomatoes or fruits (Baquero et al., 2024; Huang et al., 2020; Jiang et al., 2024; Li et al., 2024). Functional enhancements also include the incorporation of antioxidant and antimicrobial agents, as polyphenols (Sun et al., 2022; Wu et al., 2023) and  $\epsilon$ -polylysine (Li et al., 2023), to mitigate oxidation risks and inhibit microbial growth.

A key factor influencing the final properties of protein-based films is the plasticiser content used in their formulation. These compounds, such as glycerol, sorbitol, or polyethylene glycol, position themselves between polymer chains, enhancing their mobility, increasing free volume, and reducing intermolecular interactions. As a result, the material has a lower glass transition temperature, becomes easier to process, more flexible with improved elongation capacity, and has lower tensile strength. Additionally, it exhibits higher gas permeability as plasticiser content increase (Ahmad et al., 2023; Díaznez et al., 2020; García-Anaya et al., 2025; Lee et al., 2013; Osuna et al., 2022). Hydrophilic plasticisers increase the water vapour permeability of films due to their ability to interact with water, facilitating solubilization and absorption throughout the film (Ahmad et al., 2023; Pranata et al., 2019; Osuna et al., 2022). Moreover, polymer-plasticiser interactions increase the hydrophilic properties of edible films, leading to greater water solubility (Ahmad et al., 2023).

The processing set-up and storage conditions influence the conversion of OVA sulfhydryl groups into disulfide bonds, which play a very important role in forming the three-dimensional structure of the polymeric matrix, modifying the structure of the material and, consequently, the properties of the resulting EWP films (Fernández-Espada et al., 2013; González-Gutiérrez et al., 2011; Jerez et al., 2007; Jones et al., 2013; Lee et al., 2013; López-Castejón et al., 2015, 2016; Pranata et al., 2019). The manufacturing of EWP films and EWP-based composites using the solution-casting technique is usually used in recent research studies (Deng et al., 2022; Dong et al., 2022; Han et al., 2020; Huang et al., 2020; Jiang et al., 2024; Li et al., 2023, 2024; Liu et al., 2023; Zhao et al., 2020; Wu et al., 2023), however the long drying time required hinders its commercial application (Kumar et al., 2021; Weng et al., 2024). More industrial manufacturing processes have been successfully applied to produce EWP films, such as compression-moulding (Díaznez et al., 2020; González-Gutiérrez et al., 2011; Jerez et al., 2007; Lee et al., 2013), injection-moulding (Félix et al., 2014, 2017), and extrusion followed by calendaring (González-Gutiérrez et al., 2011; Pranata et al., 2019).

In addition to these factors, the properties of the films obtained from the thermo-plastic process of EWP depend on the initial characteristics of the protein (Hernández-Izquierdo and Krochta, 2008). EWP powder is widely used as a raw material and is typically produced via spray-drying, a method that is more time- and energy-efficient than

other drying technologies (Ma et al., 2021). However, spray-drying process modify the structure of the protein and its functionalities (Katekhong and Charoenrein, 2018; Lechevalier et al., 2017). The gelling properties of EWP, which are reduced after spray-drying, can be enhanced through various treatments, including dry heating. Recent research has explored the molecular interactions and gelation process of dry-heated EWP (Cheng et al., 2021; Koyama et al., 2021, 2023; Ma et al., 2022; Yuno-Ohta et al., 2021) and OVA (Koyama et al., 2024). Dry heating of EWP powder induces the formation of soluble protein aggregates (Koyama et al., 2021), the deamidation and fragmentation of the proteins (Koyama et al., 2021; Lechevalier et al., 2017), and the protein unfolding, leading to the exposure of thiol groups and hydrophobic residues. This structural modification significantly enhances the strength, transparency and water holding capacity of EWP powder gels (Cheng et al., 2021; Ma et al., 2019). These changes have been associated with a more compact gel microstructure and a significant increase in ordered secondary structures (Ma et al., 2021, 2022). Given that dry heating modifies the structure of EWP powder gels it is reasonable to hypothesize that these structural changes will also impact the properties of EWP film-forming solutions, and consequently on the properties of EWP films.

To our knowledge, the effect of the gelling capacity of dried EWP powder over the properties of EWP films has not yet been analysed. Thus, the main objective of this work was to test if the gelling capacity of EWP powder may play a role over EWP film processing and over the final characteristics of the compression-moulded EWP films. For this purpose, three commercial EWP powders based on their gelling performance were selected and characterized by determining the total soluble protein content, the relative abundance of specific proteins, the structure and morphology of the proteins, gelling capacity, and water retention capacity. Different protein-to-plasticiser ratios of the selected protein grades were prepared in order to analyse the rheological behaviour of the film-forming solutions and the mechanical, barrier, and optical properties of the EWP films obtained from the viable film-forming solutions.

## 2. Material and methods

### 2.1. Materials

For this study, 3 commercial grades of spray dried EWP powder were obtained from Bouwhuis Enthoven (Raalte, Overijssel, Netherlands), that differ in their gelling capacity: extraordinary gel (EG), high gel (HG) and low gel (LG). Food-grade glycerine (GLY) from Barcelonesa Global Chemical Solutions (Cornellà de Llobregat, Barcelona, Spain) was used as plasticiser.

### 2.2. Preparation of EWP films

Film-forming solutions (FFS) were prepared by mixing EWP powder with a mixture of glycerol and water in a 1:1 w/w ratio, using a mortar and pestle for 10 min at room temperature. Three different ratios of protein to glycerol and water were used (1:2, 1:1.5, and 1:1, denoted as a, b and c). Subsequently, the FFS were stored in the absence of oxygen under refrigeration (4 °C) for at least 24 h. Using this methodology, nine types of FFS were obtained. The EWP films were produced by compression moulding using a laboratory hot press model LP-S-50 (Labtech Engineering Co., Praksa, Muang, Samutprakarn, Thailand). A fixed amount of the FFS (10 g) was uniformly distributed between aluminium foils, and then introduced in the hot-press. The process was conducted in two cycles: the first involved applying a temperature of 130 °C and a pressure of 2.9 MPa for 5 min, followed by a cooling cycle at 2.9 MPa and 20 °C for 5 min. These conditions are similar to those used by Lee et al. (2013) to produce egg white protein films by compression moulding (128 °C, 2 MPa), and were necessary to spread completely the different film forming solutions in the mould. Then, the

EWP films were carefully removed from the aluminium foils and conditioned at 23 °C and 55 % relative humidity (RH) for at least 48 h before their use. Three replications of the FFS were elaborated for each condition, and two films from the viable FFS were obtained from each replicate.

### 2.3. EWP powder characterization

#### 2.3.1. Gel strength and water holding capacity (WHC)

Three types of egg white proteins with different gelling properties were used in the study. The EWP powder was dissolved in distilled water to prepare a dispersion at a concentration of 100 mg·mL<sup>-1</sup>. An aliquot of 15 mL was decanted into 25 mL glass beakers. The beakers were then sealed and placed in a water bath at 90 °C for 30 min to induce gelation, following the method of Ma et al. (2022). After this thermal treatment, the gels were cooled to room temperature. Subsequently, the gel strength and the water holding capacity were measured.

To characterize the gel strength, a TA-TX2 texture analyser (Stable Micro Systems, Surrey, UK) was used to perform a compression test, measuring the maximum force at which the gel breaks. A cylindrical probe with a diameter of 10 mm was employed, using a testing speed of 2 mm·s<sup>-1</sup>. The water holding capacity (WHC) of the gels was measured by cutting the gels into uniform-sized cubes and placing them in centrifuge tubes, following the method of Ma et al. (2021) with modifications. Centrifugation was performed at 8000×g for 10 min at 20 °C. The water lost by the gel was removed using filter paper. The water holding capacity (WHC) was determined as the amount of water remaining in the gel after centrifugation, using the following equation:

$$\text{WHC} = (\text{WT} - \text{Wg})/\text{WT} \times 100 \quad (1)$$

where WT is the total amount of water in the gel and Wg is the water removed in the centrifugation.

#### 2.3.2. Soluble protein content

The dried EWP powder samples were dissolved in milliQ water at 50 °C at a concentration of 100 mg·mL<sup>-1</sup> by vortex shaking for 20 min, spin centrifugation (5000×g, 1 min, 4 °C) and ultrasonic bath for 10 min at room temperature. This process was repeated 5 times and subsequently the samples were centrifuged (1500×g, 5 min, 4 °C) and the core solutions were filtered (0.45 µm PVDF syringe filters). The total soluble proteins were quantified using a Thermo Scientific™ Pierce™ Detergent Compatible Bradford assay kit based on a colorimetric method that uses Coomassie as a reagent (López-Mata et al., 2016). Absorbance was measured at 595 nm after 10-min incubation of the reagent (300 µL) with the sample (10 µL) at room temperature. A bovine serum albumin standard curve was built (R<sup>2</sup>=0.9957). The analysis was performed by triplicate and the data were expressed as soluble protein content (%).

#### 2.3.3. Fourier transform infrared (FTIR) spectroscopy

The infrared spectra of the EWP powders were recorded using an ATR-FTIR Alpha spectrometer (Bruker Corporation, Billerica, Massachusetts, USA) over the range of 4000–400 cm<sup>-1</sup>, with 128 scans at 1 cm<sup>-1</sup> resolution. The FTIR spectra data were normalized, Gaussian deconvoluted, and second derivative fitted between 1700 and 1600 cm<sup>-1</sup> using OriginPro v24b software (OriginLab, Northampton, Massachusetts, USA). Quantitative estimation of secondary structure components was performed using Gaussian peaks and curve fitting models according to the procedure of Susi and Byler (1983).

#### 2.3.4. X-ray diffraction (XRD)

EWP powder samples were analysed using a PANalytical Empyrean X-ray diffractometer (Malvern Panalytical, Malvern, Worcestershire, United Kingdom). A monochromatized CuK<sub>α</sub> radiation (λ = 1.5406 Å) at 45 kV and 40 mA was used over a scanning range (2θ) from 4° to 90° with a step size of 0.0131°, and a counting time of 0.552 s·step<sup>-1</sup> (Kang

et al., 2016).

#### 2.3.5. Liquid chromatography-electrospray ionization-tandem mass spectrometry (LC-ESI-MS/MS)

The previously dissolved samples underwent an enzymatic digestion process: the samples were aliquoted into 0.5 mL microtubes, with each fraction containing 20 µg of total protein, evaporated and resuspended in 10 µL of denaturing buffer (6 M urea, 100 mM Tris pH 8). The disulfide bonds were reduced with 1.5 µL of 200 mM Dithiothreitol (DTT) for 30 min at 37 °C. After this, 6 µL of 200 mM iodoacetamide was added, and solutions were stored for 30 min in darkness. Later on, 6 µL of reducing agent (DTT 200 mM) was added. After 30 min at room temperature, the samples were diluted to a final concentration of <1 M urea with ammonium bicarbonate (50 mM). Digestion reaction was carried out overnight at 37 °C with the trypsin enzyme (Gold Trypsin, Promega) at an enzyme-to-protein ratio of 1:20. The reaction was stopped by adding concentrated formic acid (FA). Finally, samples were evaporated and resuspended in 2 % acetonitrile (ACN), 0.1 % FA, and filtered through 0.45 µm PVDF filters.

Proteins (500 ng) were identified on a hybrid triple quadrupole/linear ion trap mass spectrometer (6500QTRAP+, Sciex, Foster City, CA, USA) coupled to a nano/micro-HPLC (Eksigent LC425, Sciex). Samples preconcentration and desalting was performed using a C18 precolumn (Luna® 0.3 mm id, 20 mm, 5 µm particle size, Phenomenex, CA, USA) at 10 µL·min<sup>-1</sup> for 3 min. Peptide separation was performed using a C18 column (Luna® 0.3 mm id, 150 mm, 3 µm particle size, Phenomenex, CA, USA) at 5 µL·min<sup>-1</sup>, and column was maintained at 40 °C. The elution gradient was from 3 % to 30 % ACN (0.1 % FA) in 30 min.

The mass spectrometer was interfaced with an ESI source (Turbo V™) using a 25 µm ID hybrid electrode and operated in positive mode. The source parameters were: capillary voltage 5 kV, declustering potential 85 V, and ion source gas (nitrogen) at 15 psi.

Protein identification was carried out using the Mascot search engine (Matrix Science; London, UK) with public protein sequence databases (Swissprot, NCBI) according to *Gallus gallus* taxonomy. The relative abundance of the identified proteins was estimated by calculating the exponentially modified protein abundance index (emPAI), which allows gaining insight into proteome profiles without the need to perform quantification with standard synthetic peptides (Ishihama et al., 2005).

### 2.4. FFS characterization

The rheological behaviour of FFS was measured using a MCR301 rheometer (Anton Paar Physica, Graz, Austria) equipped with serrated parallel plate geometry (50 mm diameter, 1 mm gap). Prior to analysis, the samples were brought to room temperature. The shear stress (τ) curves were obtained from rotational tests for shear rates (γ̇) over a range of 0.01 to 100 s<sup>-1</sup> for 7.5 min (Liu et al., 2024). The data were fitted to the Power law model:

$$\tau = K \cdot \dot{\gamma}^n \quad (2)$$

where *K* is the consistency index (Pa·s<sup>*n*</sup>) and *n* is the flow index.

To determine the effect of temperature on the viscosity of FFS, rotational tests at a heating rate of 5 °C·min<sup>-1</sup> from 25 °C to 130 °C were performed at a shear rate of 50 s<sup>-1</sup> (selected to guarantee the existence of a linear range according to shear rate sweeps carried out previously). Before starting the heating ramp, the samples were held at 25 °C for 4 min at steady state followed by 1 min at a shear rate of 10 s<sup>-1</sup>. To minimize evaporation during the heating process, an accessory with silicone oil was used.

Oscillatory shear tests at 20 °C were conducted to determine the viscoelastic properties of the FFS. Frequency sweep tests were performed from 0.1 to 100 Hz at a constant strain of 0.1 % (selected from strain sweep tests to ensure linear behaviour) to obtain the storage and loss moduli (Pa). The rheological measurements were performed from 3

batches of FFS.

## 2.5. EWP films characterization

The FTIR spectra and XRD patterns of the EWP films were obtained as previously described for EWP.

### 2.5.1. SEM

EWP films were prepared by freeze-fracturing after immersion in liquid nitrogen. The fractured samples were mounted on a stub using conductive carbon tape and coated with Palladium (14 nm). Surface morphology and cross-sections were analysed using a field-emission scanning electron microscope (SEM) INSPECT-F50 (Thermo Fisher Scientific, Waltham, Massachusetts, USA) operated at an accelerating voltage of 10 kV.

### 2.5.2. Mechanical properties

Tensile strength (TS), elongation at break (EAB), and Young's modulus (E) were measured using a texture analyser TA-XT2i (Stable Micro System Ltd, Godalming, UK) equipped with A/TGR grips, following the ASTM D882–18 standard method (ASTM, 2018). The films were cut into rectangular strips (10 mm width x 90 mm length) and conditioned for 48 h at 23 °C and 50 % RH. The tensile tests were conducted at a speed of 1 mm·s<sup>-1</sup> and with a gap between grips of 50 mm. The TS (MPa) was obtained by dividing the maximum load (N) for breaking the film by the initial cross sectional area (mm<sup>2</sup>), EAB (%) was calculated as the percentage increase in length of the sample at rupture, and E (MPa) was calculated by dividing TS by the tensile strain at rupture (the ratio of the elongation distance to the initial length of the film).

To complement the mechanical characterization, multi-axial deformation tests and puncture test were conducted using the HDP/FSR film support rig probe (Stable Micro System Ltd, Godalming, UK). For the multi-axial deformation tests, a SMS 9/5S cylindrical probe with a 5 mm diameter was used, while a P/2 N needle probe was used for the puncture test (Stable Micro System Ltd, Godalming, UK). In both tests, the speed was 0.10 mm·s<sup>-1</sup> and the penetration distance was 5 mm. The results were expressed in terms of maximum force (N). For each processing conditions, five samples of three films replicas were tested.

### 2.5.3. Optical properties

The colour of the films was determined using a colorimeter CR-200 (Konica Minolta Sensing INC., Tokyo, Japan). The measurements were performed in the CIELAB colour space, where L\* corresponds to luminance-darkness (expressed as a percentage), a\* represents the red (positive) and green (negative) hues, and b\* represents the yellow (positive) and blue (negative) hues. The assessments were performed on the white reflector plate of the colorimeter. The transmittance of the films was measured using a Libra S22 spectrophotometer (Biochrom Cambridge, United Kingdom) at a wavelength of 600 nm. The films were cut in strips (25 mm × 10 mm) and fixed into the cuvette surface. For reference, an emptied cuvette was used. For each processing conditions, two measures of three films replicas were tested.

### 2.5.4. Oxygen permeability (OP) and water vapour permeability (WVP)

The oxygen transmission rates (OTR) of the different films were measured according to the standard ASTM D3985–17 (ASTM, 2017) using a MOCON Ox-Tran® Model 2/22 (Minneapolis, USA), while the water vapour transmission rates (WVTR) were measured following the standard ASTM F1249–20 (ASTM, 2020) using a MOCON Permatran-W® Model 3/34 (Minneapolis, USA). All analyses were performed at 23 °C and 50 % RH. At least one measurement in each of the 6 films obtained per condition was performed. Both oxygen and water vapour permeability,  $P$  (kg·m<sup>-2</sup>·s<sup>-1</sup>·Pa<sup>-1</sup>), were calculated from the corresponding transmission rates,  $TR$  (kg·m<sup>-2</sup>·s<sup>-1</sup>), using the following equation:

$$P = \frac{TR \cdot e}{\Delta P} \quad (3)$$

where  $e$  is the mean film thickness (m), measured in 5 points with a digital thickness gauge (model 547–401, Mitutoyo, Japan), and  $\Delta P$ (Pa) is the partial pressure difference of oxygen or water vapour.

## 2.6. Statistical analysis

Data are presented as the mean value ± standard deviation (SD). One-way analysis of variance (ANOVA) followed by Tuckey's post hoc test for comparison of means was conducted. Statistical analysis was performed using GraphPad Prism version 10 (GraphPad Software, San Diego, CA). Differences were considered significant at  $p < 0.05$ . Data were also evaluated using Pearson's correlation analysis to examine the relationships between the parameters characterizing EWP, the rheological properties of the film-forming solution, and the properties of the resulting films.

## 3. Results and discussion

### 3.1. Characterization of EWP

#### 3.1.1. Gel strength and water holding capacity (WHC)

The protein with the highest claimed gelation capacity (EG) exhibited the greatest gel hardness (11.82 ± 1.66 N), whereas the protein with the lowest claimed gelation capacity (LG) had the lowest gel hardness (5.13 ± 0.29 N) (Table S1). No significant differences were observed between the EG and HG samples, while significant differences ( $p < 0.05$ ) were found when compared to the LG sample. The water holding capacity (WHC) followed a similar pattern to gel hardness, as no differences ( $p > 0.05$ ) were detected between the EG and HG samples (91.40 ± 0.51 % and 91.93 ± 0.16 %, respectively), whereas the LG sample showed a significantly ( $p < 0.05$ ) lower value (83.72 ± 2.39 %) compared to the other samples (Table S1). The gelation capacity and water-holding ability vary depending on the dry-heating conditions of powdered EWP. The partial unfolding of the native conformation induced by dry-heating leads to the exposure of buried functional groups, facilitating protein-protein interactions and enhancing gelation properties (Cheng et al., 2021; Ma et al., 2019).

#### 3.1.2. Soluble protein content

The Bradford assay results revealed soluble protein contents of 47.11 ± 1.25, 55.69 ± 0.78 and 40.65 ± 0.34 for EG, HG and LG, respectively (Table S1). This indicates that LG, the EWP with the lowest gelling power, had the lowest soluble protein content, and more intense thermal treatments applied to obtain EG and HG grades had a significant impact over soluble protein content. Effectively, has been demonstrated that the dry-heating may induce protein denaturation and EWPs forming soluble protein aggregates, and these aggregates are key to improve the gelling properties of egg white proteins (Koyama et al., 2023; 2024).

#### 3.1.3. FTIR

The FTIR spectra of the three types of EWP powder is shown in Fig. 1a. All samples exhibited characteristic amide transmittance bands, clearly located at the same wavenumber section, specifically: amide A (3272 cm<sup>-1</sup>), amide B (2961 cm<sup>-1</sup>), amide I (1632 cm<sup>-1</sup>), amide II (1516 cm<sup>-1</sup>), and amide III (1392 cm<sup>-1</sup>). The obtained data match the absorption ranges of the protein's functional groups reported by Barth (2007).

The quantitative results for changes in the secondary structure of the EWP powder by curve-fitting analysis in the amide I region are shown in Fig. 1b. According to Susi and Byler (1983), bands in the regions of 1650–1658 cm<sup>-1</sup>, 1610–1640 cm<sup>-1</sup>, 1660–1700 cm<sup>-1</sup> and 1640–1650 cm<sup>-1</sup> were assigned to  $\alpha$ -helix,  $\beta$ -sheet,  $\beta$ -turn and unordered, respectively. Overall, the egg white protein samples had a higher proportion of

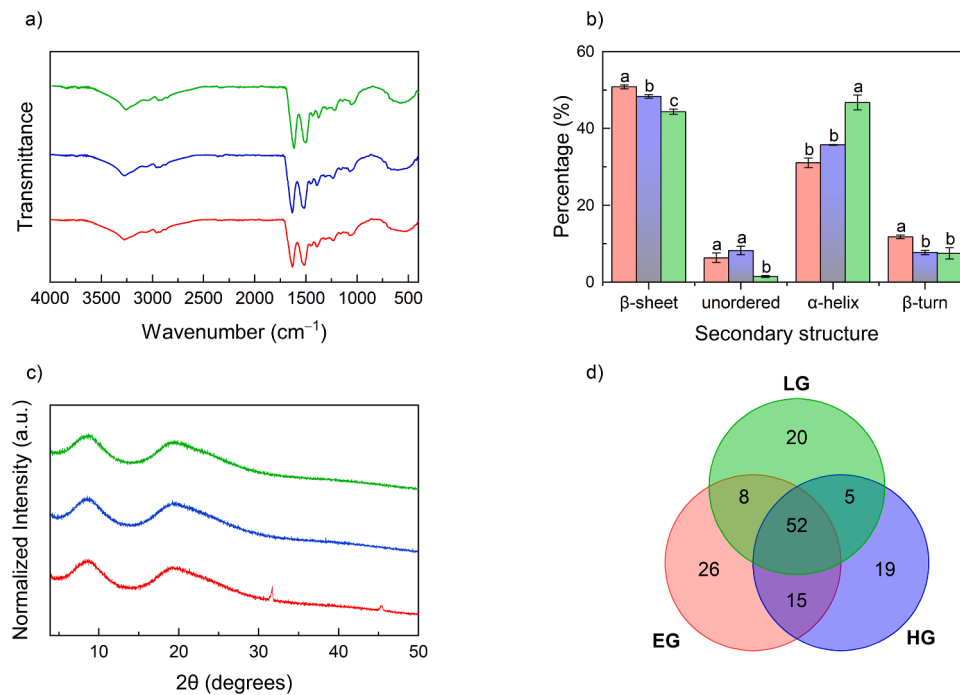


**Fig. 1.** FTIR spectra (a), Secondary structure (b), X-ray diffraction patterns (c), and Venn diagram of proteins identified by LC-ESI-MS/MS (d) for different EWP: EG (red), HG (blue) and LG (green). Different letters for the same secondary structure indicate significant differences between EWP ( $p < 0.05$ ).

$\beta$ -sheets and  $\alpha$ -helices compared to  $\beta$ -turns and unordered structures, suggesting that a folded conformation predominates in these proteins. The EWP grade with the highest gelation capacity (EG) exhibited a greater proportion of  $\beta$ -sheets and  $\beta$ -turns (50.85 % and 11.77 %, respectively) compared to HG (48.35 % and 7.70 %) and LG (44.34 % and 7.48 %). Conversely, the  $\alpha$ -helices followed an opposite trend: the EG sample had the lowest percentage of  $\alpha$ -helices (31.07 %), while the LG sample displayed the highest value (46.74 %).  $\beta$ -sheets are commonly associated with strong intermolecular interactions due to their ability to form hydrogen-bonded networks, which enhance gelation by imparting structural rigidity and stability to the gel matrix. A positive correlation between the  $\beta$ -sheets content and the hardness of protein gels has been reported in previous studies (Su et al., 2015; Wei et al., 2018; Yao et al., 2024).

### 3.1.4. XRD

The XRD patterns (Fig. 1c) indicated that the three EWP samples had an amorphous structure due to the broad of the peaks (Deng et al., 2022). EWP powders exhibited two broad peaks at  $2\theta = 8.5^\circ$  and  $19^\circ$  corresponding to  $\alpha$ -helix and  $\beta$ -sheet structures of the protein's secondary conformation, respectively (Deng et al., 2022; Kang et al., 2016). However, two sharper peaks, located at  $2\theta = 31.6^\circ$  and  $45.4^\circ$ , appeared in the EG sample, which were not present in the other two types of EWP, and may be assigned to impurities present in the sample. These peaks were described previously as NaCl fragments in egg albumen gels dried (Tian et al., 2018).

### 3.1.5. LC-ESI-MS/MS identification

A total of 145 protein identifications (ions score  $>37$ ) were reported in the LC-ESI-MS/MS analysis performed to the three EWP powder grades. Among them, 52 protein identifications were in common for all grades (Fig. 1d), and exclusive identifications were found for EG (26), HG (19), and LG (20), indicating that each EWP grade has a different protein profile. All identifications can be summarized in 15 effective proteins, including the main proteins in egg whites (OVA, ovotransferrin and ovomucoid).

As expected, OVA and ovotransferrin were the proteins with the

highest emPAI values, indicating greater relative abundance in the samples. Specifically, the sums of the emPAI values for common OVA identifications in EG, HG and LG were 309.6, 299.6, and 201.3, respectively (Table S2). Similarly, the sums of the emPAI values for ovotransferrin identifications in EG, HG and LG were 178.5, 118.1 and 60.2, respectively. In addition, several OVA fragments with slightly lower molecular weights than native OVA, along with OVA-related proteins, were identified in all samples. These differences in the soluble protein fraction identifications among the grades of EWP powders could be attributed to the distinct processing conditions applied to produce EWP with different gel forming capacities (spray-drying plus heat treatment). During dry heating, EWP forms soluble protein aggregates in which covalent and disulfide bonds are involved. Forming soluble aggregates via covalent bonds is key to enhancing the gelling properties of EWP (Koyama et al., 2023; 2024). Additionally, dry heating induces fragmentation, as observed in sodium dodecyl sulfate-polyacrylamide gel electrophoresis (SDS-PAGE) analysis of dry-heated EWP as a 10 kDa band (Lechevalier et al., 2017; Koyama et al., 2021). Furthermore, smaller molecular weight fragments compared to the monomer were detected in dry-heated OVA (Koyama et al., 2024). Interestingly, lysozyme was only detected in HG and LG samples. Probably, a more intense heat treatment applied to obtain EG grade fragmented or modified significantly this protein, not being able to be detected by LC-ESI-MS/MS. Effectively, previous studies have demonstrated that lysozyme is very heat-labile and gets degraded by heat treatments (Shin et al., 2013). Other major proteins, such as ovomucoid and ovomucin, were also detected in the three samples of EWP powder. In addition, minor proteins present in egg whites were identified: ovoinhibitor, ovoglycoprotein, ovomacroglobulin or ovo-flavoprotein, among others.

## 3.2. Rheological behaviour of FFS

FFS with a 1:1 protein to plasticiser ratio became excessively hard when formulated with EG protein, whereas mixtures with a 1:2 ratio exhibited phase separation after the stabilization period in the HG and LG protein cases. Consequently, the rheological properties of these

samples could not be assessed.

The steady shear behaviour of the film-forming solution was analysed to understand the processability of the non-discarded mixtures. The flow properties of the solution have a significant impact on the thickness, spreadability, and uniformity of the resulting film (Chen et al., 2009; Liu et al., 2024; Sun et al., 2020). Fig. 2a shows the variation of shear stress ( $\tau$ ) with the shear rate ( $\dot{\gamma}$ ) obtained from rotational tests. The FFS demonstrated typical pseudoplastic behaviour, characterised by a reduction in apparent viscosity as shear rate increased, attributed to the alignment of the microstructure in the flow direction. The experimental data were fitted to the power-law equation (Eq. (2)), achieving coefficients of determination ( $R^2$ ) higher than 0.987 (Table 1). All FFS exhibited a shear-thinning behaviour, with flow index ( $n$ ) values significantly deviating from 1, indicating a non-Newtonian behaviour. This effect was previously reported for protein FFS due to the destruction of entanglement between molecules under high-speed shear (Liu et al., 2024; Peña-Cháidez et al., 2021; Sun et al., 2020). FFS showed increasing  $n$  values and decreasing consistency index ( $K$ ) values as the plasticiser content rose. Viscosity decreased with increasing shear rate until stabilising at an approximately constant value beyond  $80 \text{ s}^{-1}$ . Table 1 presents the initial viscosity and the viscosity at  $80 \text{ s}^{-1}$ . For identical protein-to-plasticiser ratios, viscosity increased with the protein's gelling capacity. Similarly, for a given type of EWP powder, higher protein proportions in the mixture resulted in increased viscosity. This behaviour was described for other protein-based FFS and could be due to the plasticiser weakening the intermolecular or intramolecular forces of EWP. As a result, the tightly organized polymer network structure was disrupted by the plasticiser, leading to the formation of new hydrogen bonds between the polymers (Sun et al., 2020; Verbeek and van den Berg, 2010). These findings align with the observed inability to process EG protein mixtures at a 1:1 ratio.

The temperature-dependent viscosity of the FFS is shown in Fig. 2b. From  $25 \text{ }^\circ\text{C}$  to  $70 \text{ }^\circ\text{C}$ , viscosity declined. Beyond  $70 \text{ }^\circ\text{C}$ , viscosity increased across all formulations due to the onset of gelation, driven by protein denaturation, unfolding, and subsequent aggregate formation via hydrophobic interactions and sulfhydryl–disulfide bonding (Cheng et al., 2021; Ma et al., 2022). This coagulation and branching restrict molecular movement, leading to higher viscosity (Rouilly et al., 2006).

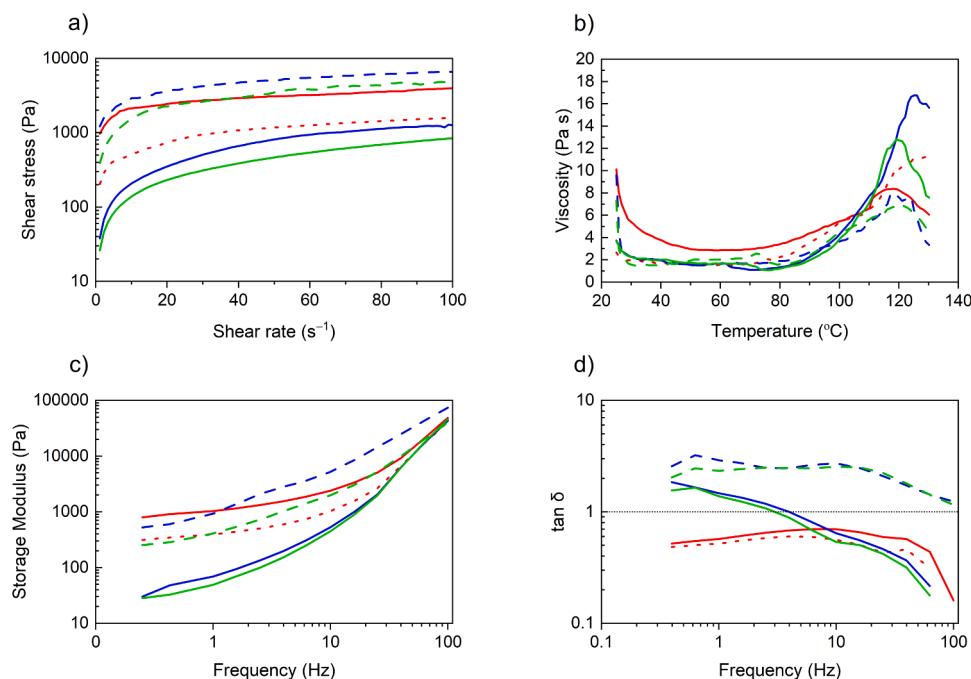


Fig. 2. Flow curve (a), variation of viscosity with temperature (b), storage modulus (c), and loss factor ( $\tan \delta$ ) (d) in film-forming solutions elaborated with different EWP and protein/plasticiser ratios (··· EGa; — EGb; - - HGb; — HGc; - - LGb; — LGc).

Table 1

Power law model constants, consistency index ( $K$ ), flow index ( $n$ ), coefficient of determination ( $R^2$ ), initial viscosity ( $\eta_0$ ) and viscosity ( $\eta$ ) at a shear rate of  $80 \text{ s}^{-1}$ , for film-forming solutions (FFS) derived from different EWP (EG, HG, and LG) and protein/plasticiser ratios of 1:2 (a), 1:1.5 (b), and 1:1 (c). The values are means  $\pm$  standard deviation of the replicates. The values followed by different letters in the same column are significantly different according to the Tuckey's test ( $p < 0.05$ ).

FFS Sample	$K$ (Pa·s <sup>n</sup> )	$n$	$R^2$	$\eta_0$ (Pa·s)	$\eta$ at $80 \text{ s}^{-1}$ (Pa·s)
EGa	190.36 $\pm 2.73^c$	0.462 $\pm 0.003^c$	0.997	180.93 $\pm 9.72^c$	$17.97 \pm 3.32^b$
EGb	1053.88 $\pm 17.04^e$	0.278 $\pm 0.004^a$	0.987	858.78 $\pm 5.37^e$	$44.47 \pm 4.19^c$
HGb	38.95 $\pm 1.63^b$	0.766 $\pm 0.010^e$	0.993	33.54 $\pm 4.34^b$	14.12 $\pm 1.73^{ab}$
HGc	1164.19 $\pm 5.77^f$	0.379 $\pm 0.001^b$	0.999	1077.42 $\pm 45.64^f$	76.63 $\pm 11.23^d$
LGb	19.36 $\pm 0.34^a$	0.816 $\pm 0.004^f$	0.999	23.05 $\pm 2.61^a$	$8.65 \pm 2.48^a$
LGc	476.98 $\pm 12.60^d$	0.508 $\pm 0.006^d$	0.992	343.19 $\pm 26.76^d$	54.64 $\pm 18.01^{cd}$

Given the relative abundance of ovotransferrin and OVA in powdered EWP samples, gelation will primarily depend on these proteins. Ovotransferrin plays a key role in initiating denaturation, due to its lower denaturation temperature ( $65 \text{ }^\circ\text{C}$ ) compared to OVA ( $84.5 \text{ }^\circ\text{C}$ ) (Li-Chan et al., 2007; Strixner and Kulozik, 2011).

The evolution of storage modulus and loss factor with frequency for the different FFS, derived from oscillatory tests, is depicted in Fig. 2c and 2d, respectively. Both storage and loss moduli increased substantially with higher protein-to-plasticiser ratios, in agreement with other studies (Fernández-Espada et al., 2013; Sobral et al., 2005; Sun et al., 2020). FFS formulated with EG proteins exhibited a storage modulus exceeding the loss modulus ( $\tan \delta < 1$ ) across all frequencies, indicating predominantly elastic behaviour. Conversely, HG- and LG-based formulations showed a viscous character, with loss modulus surpassing storage modulus ( $\tan \delta > 1$ ) at all oscillatory frequencies when the protein-to-plasticiser ratio was 1:1. At a 1:1.5 ratio, the moduli

intersected, and the FFS transitioned from viscous to elastic behaviour above 4 Hz. At higher frequencies, the slope of both viscoelastic functions increased for 1:2 and 1:1.5 ratios. However, higher protein concentrations enhanced material structuring through increased covalent bonding, resulting in minimal slope changes. For a given protein-to-plasticisers ratio, both moduli displayed higher values with stronger gelling proteins, with differences particularly notable in EG protein formulations. It is difficult to compare the evolution of the loss factor with frequency with that obtained in other protein-based film-forming solutions, as it depends on the type of protein and composition of the FFS. There are cases where a transition from viscous to elastic behaviour occurs (Sun et al., 2020), and cases where  $\tan \delta < 1$  throughout the entire frequency or strain range (Peña-Cháidez et al.,

2021; Sobral et al., 2005; Yuno-Ohta et al., 2021).

### 3.3. Influence of the protein-to-plasticisers ratio and gelling power on EWP films properties

#### 3.3.1. Morphological properties of EWP films

The surface and cross-sectional morphology of the EWP films obtained was analysed by SEM (Fig. 3). The SEM images of the film surfaces showed in EGa and HGc a few white spots, while in HGb and LGb samples the number of this white spots was significant. Thus, in HGb and LGb films was not possible to obtain homogeneous and defect-free areas, so were discarded for the evaluation of the mechanical properties. The presence of these white spots may be attributed to the generations of

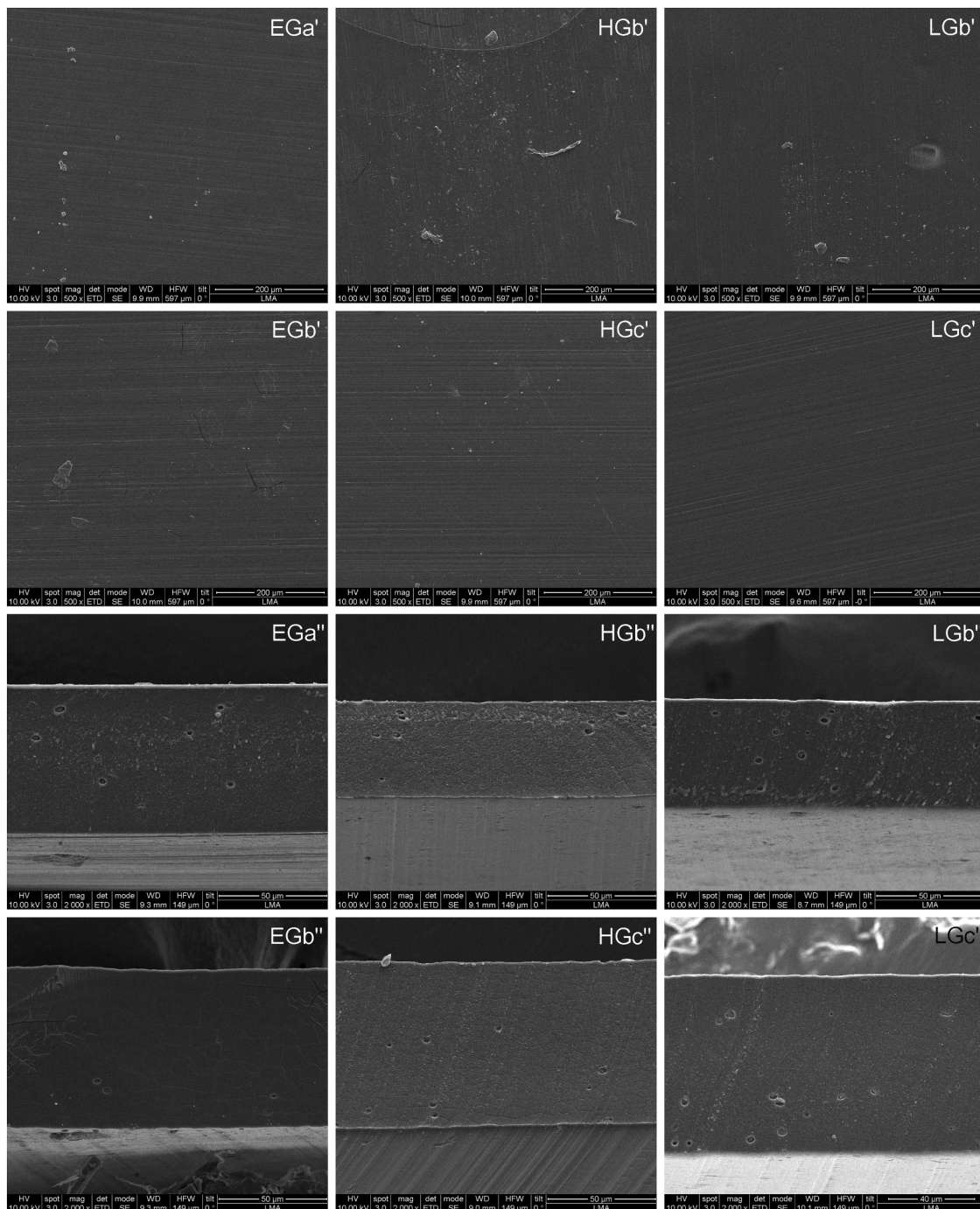


Fig. 3. SEM images of the film surfaces (denoted by ') and film cross-sections (denoted by ") developed with different EWP and protein/plasticiser ratios.

clusters of highly concentrated aggregated proteins, resulting from the non-homogeneous mixing of certain parts of the protein network with the plasticisers, as previously described by Lee et al. (2013) in EWP films. Moreover, as can be observed in the images, the thickness of the defect-free areas of these films is lower:  $72.67 \pm 4.66 \mu\text{m}$  for HGb and  $68.77 \pm 6.71 \mu\text{m}$  for LGb. In the rest of the films, the thickness ranged between 90.37 and 93.63  $\mu\text{m}$ . In some samples, such as EGb, some cracks were observed. This may be due to the sample preparation, as vacuum generation may cause some of the moisture to be lost, or to degradation caused by the electron beam of the microscope, a phenomenon that has occurred previously in soy protein films produced by compression moulding (Ogale et al., 2000).

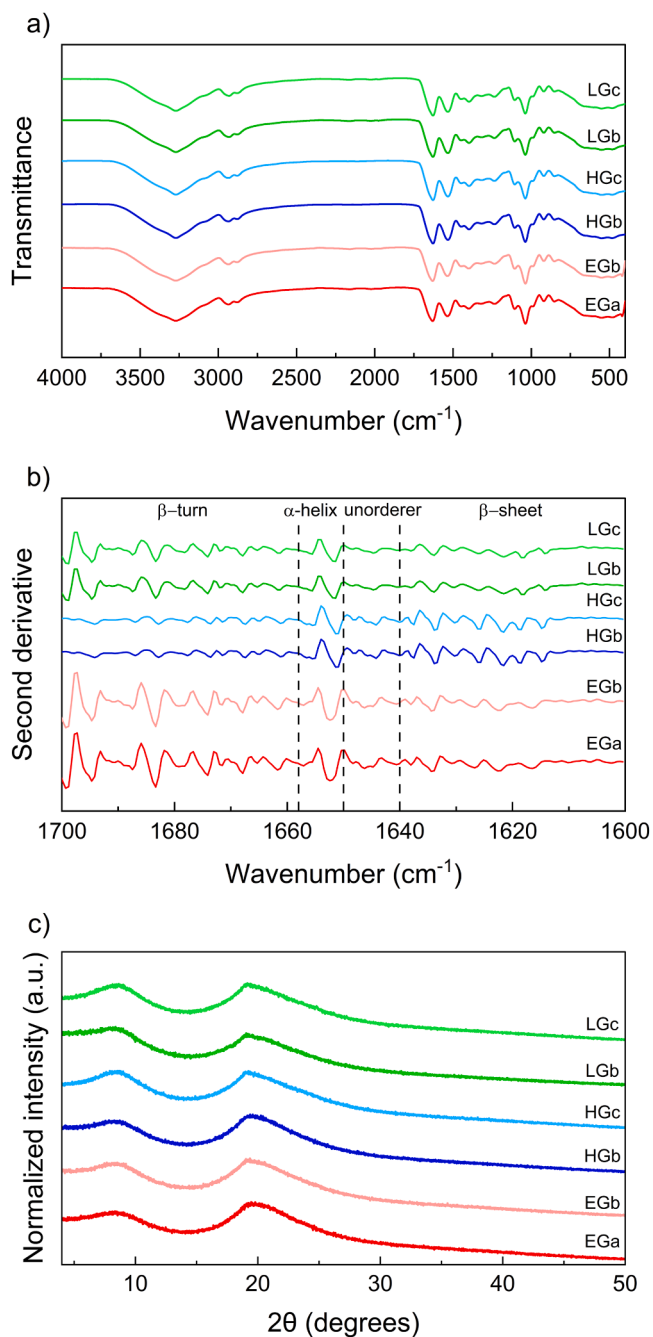


Fig. 4. FTIR spectra (a), Second derivative (b), and X-ray diffraction patterns (c) for different EWP films: EG (red), HG (blue) and LG (green).

### 3.3.2. FTIR and XRD of EWP films

The FTIR spectra of EWP films with different proteins and protein-to-plasticiser ratios are shown in Fig. 4a. All the films produced exhibited similar spectra and were comparable to those previously obtained for EWP powder (Fig. 4a). As expected, peaks corresponding to amine A, amine I, amine II, and amine III were observed. However, additional peaks appeared in the FTIR spectra of the proteins at  $1035 \text{ cm}^{-1}$  and  $630 \text{ cm}^{-1}$ , which can be attributed to the presence of glycerol as a plasticiser (Deng et al., 2022; Li et al., 2024).

In order to identify the main components that contribute to the amide I band of EWP films, the second derivative was calculated and displayed in Fig. 4b. Films made of EG protein showed a greater intensity of the bands located in  $1650\text{--}1658 \text{ cm}^{-1}$  and  $1660\text{--}1700 \text{ cm}^{-1}$  regions, related with  $\alpha$ -helix and  $\beta$ -turns structures, compared with films made of LG and HG proteins. However, differences in  $1610\text{--}1640 \text{ cm}^{-1}$  and  $1640\text{--}1650 \text{ cm}^{-1}$  regions, related with  $\beta$ -sheet and unordered structures, were less evident. No differences were observed between films based on the same raw protein.

The XRD patterns (Fig. 4c) of EWP films with different proteins and protein-to-plasticisers ratios provided an amorphous structure, with two broad peaks at  $2\theta = 8.5^\circ$  and  $19^\circ$ , as previously observed in the protein powder (Fig. 1c). Other authors have described the same XRD patterns with the two broad peaks in EWP films (Jiang et al., 2024; Li et al., 2024)

### 3.3.3. Mechanical properties of EWP films

The tensile strength of EWP films (Fig. 5) ranged from  $2.56 \pm 0.81 \text{ MPa}$  in EGa samples to  $7.91 \pm 1.15 \text{ MPa}$  in HGc samples. This wide range of values may be attributed to the protein-to-plasticiser ratio, since tensile strength in EGb samples ( $4.21 \pm 0.78 \text{ MPa}$ ) was significantly higher than in EGa samples ( $2.56 \pm 0.81 \text{ MPa}$ ), for the same EWP. Although samples with a higher protein-to-plasticiser ratio are not comparable with those with a smaller ratio, since the EWP utilized is different, it is worth to remark that the tensile strength was significantly higher in these ones. This can be attributed to the lower percentage of glycerol in these formulations and/or the lower gel strength of the powdered EWP used in these samples (HGc, LGc). However, no significant differences were found in the tensile strength between films made with different EWP grade but with the same protein-to-plasticiser ratio: HGc ( $7.91 \pm 1.15 \text{ MPa}$ ) and LGc ( $7.66 \pm 1.82 \text{ MPa}$ ). The tensile strength values were similar to those reported by other authors for compression moulded EWP films and similar glycerol content (Lee et al., 2013; González-Gutiérrez et al., 2010). Furthermore, the role of the protein-to-plasticiser ratio on the tensile strength of films has been previously described for protein films and protein-based composites (Ahmad et al., 2023; Díaz et al., 2020; García-Anaya et al., 2025; Liu et al., 2022; Lee et al., 2013; López-Castejón et al., 2015; Osuna et al., 2022; Sun et al., 2020). This effect can be explained by the fact that glycerol, acting as a plasticiser, integrates itself between polymer chains, restricting hydrogen bonds formation and increasing intermolecular space. This led to greater chain mobility, a reduction in intermolecular stress and a decrease in tensile strength (Díaz et al., 2020; Liu et al., 2022; Osuna et al., 2022). Although the parameter most strongly correlated with the mechanical properties of the films is the protein-to-plasticiser ratio, the tensile strength of EWP films is also related to the secondary structure of the proteins used in the formulation, particularly the  $\beta$ -turn content, as shown in the correlation analyses carried out between the parameters characterizing the structural properties of EWP and films, the rheological properties of the FFS, and the properties of the resulting films (Fig. 6).

The modulus of elasticity (E) of the obtained EWP films (Fig. 5) ranged from  $5.17 \pm 2.16 \text{ MPa}$  in EGa samples to  $12.91 \pm 4.44 \text{ MPa}$  in LGc samples. As with tensile strength, the protein-to-plasticiser ratio may be the responsible of such variability. Samples with higher plasticiser content and those made with EWP of greater gelling capacity exhibited a lower modulus of elasticity. These results are aligned with previous studies on EWP and other protein-based films, where an

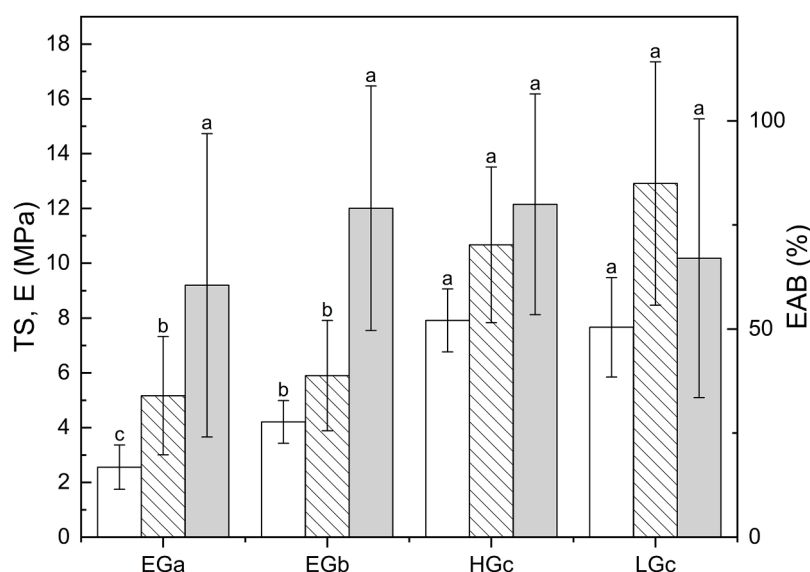


**Fig. 5.** Tensile strength (TS, white), elastic modulus (E, striped) and elongation at break (EAB, grey) of films developed with different EWP and protein/plasticiser ratios. Data are presented as mean values, and error bars indicate standard deviation ( $n = 15$ ). Different letters for the same parameter indicate significant differences between films ( $p < 0.05$ ).

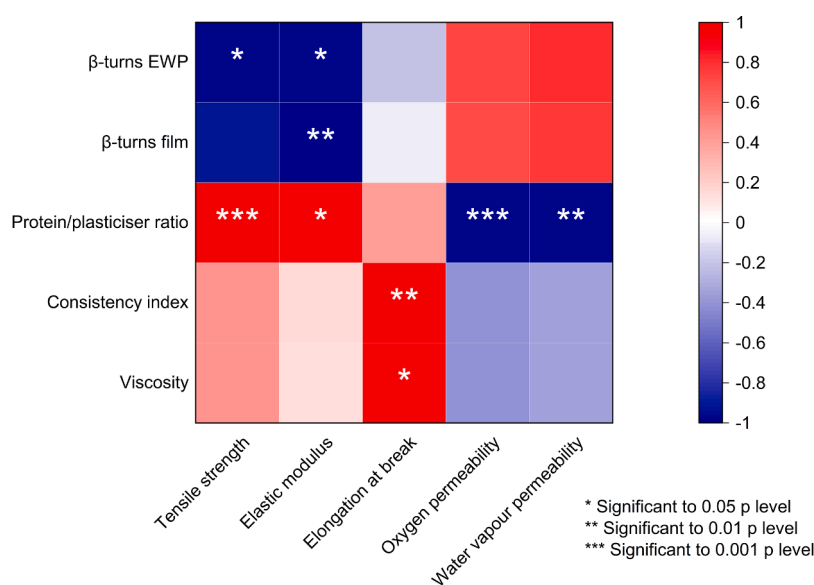


**Fig. 6.** Correlations between the structural characteristics of the EWP and EWP film, and the mechanical and permeability properties of the obtained EWP films.

increase in plasticiser content similarly reduced E values (Ahmad et al., 2023; García-Anaya et al., 2025; Lee et al., 2013; Osuna et al., 2022). Lee et al. (2013) attributed this behaviour to the increase in free volume, which causes a restructuration of the polymer matrix, reducing the stiffness. The modulus of elasticity of EWP films is related to the  $\beta$ -turn structures content in the EWP ( $p < 0.05$ ) and in the EWP films ( $p < 0.01$ ) (Fig. 6). Effectively, the increase of  $\beta$ -turn structures may have important implications on the flexibility of the protein film (Proaño et al., 2020).

The elongation at break (EAB) of EWP films ranged from 60.51 % to 79.95 % (Fig. 5), with no significant differences ( $p > 0.05$ ) observed either between protein types or across different plasticiser contents. However, other authors have noted that glycerol enhances polymer mobility and, therefore, can improve the elongation at break of protein-based and composite films (García-Anaya et al., 2025; Liu et al., 2022; Osuna et al., 2022). The EAB values were higher than those reported for EWP films produced using other methods, such as casting or extrusion

and calendering (Deseta et al., 2023; Huang et al., 2020; Liu et al., 2023; Pranata et al., 2019) but slightly lower than those obtained for EWP sheets formed by compression moulding (Lee et al., 2013).

The results obtained from the multi-axial deformation and puncture tests (Figure S1) were aligned with the results obtained from the tensile tests, showing an increase of the multi-axial and puncture maximum force as the protein to plasticiser ratio was increased. However, no apparent effect of the EWP grade was detected.

### 3.3.4. Optical properties

The values of CIELAB coordinates ( $L^*$ ,  $a^*$ ,  $b^*$ ) and transmittance are showed for the different EWP films in Table 2. The luminosity,  $L^*$ , of all the films was between 95.94 and 96.47, the coordinate  $a^*$  between  $-0.39$  and  $-0.67$ , and the coordinate  $b^*$  between 3.05 and 3.91, with no significant differences ( $p > 0.05$ ) between films. These values were comparable to those obtained by Pranata et al. (2019) for EWP films produced by extrusion and calendering, and conditioned at 23 °C at 55

**Table 2**

CIELAB color coordinates ( $L^*$ ,  $a^*$ , and  $b^*$ ) and transmittance of EWP films developed with different EWP (EG, HG, and LG) and protein/plasticiser ratios of 1:2 (a), 1:1.5 (b), and 1:1 (c). The values are means  $\pm$  standard deviation of the replicates ( $n = 6$ ). The values followed by different letters in the same column are significantly different according to the Tuckey's test ( $p < 0.05$ ).

Film Sample	$L^*$	$a^*$	$b^*$	Transmittance (%)
EGa	96.40 $\pm$ 0.87 <sup>a</sup>	-0.47 $\pm$ 0.28 <sup>a</sup>	3.54 $\pm$ 0.96 <sup>a</sup>	78.43 $\pm$ 4.72 <sup>a</sup>
EGb	96.32 $\pm$ 0.72 <sup>a</sup>	-0.58 $\pm$ 0.26 <sup>a</sup>	3.84 $\pm$ 0.81 <sup>a</sup>	78.86 $\pm$ 3.29 <sup>a</sup>
HGb	95.94 $\pm$ 0.58 <sup>a</sup>	-0.67 $\pm$ 0.22 <sup>a</sup>	3.91 $\pm$ 0.60 <sup>a</sup>	79.28 $\pm$ 4.04 <sup>a</sup>
HGc	96.47 $\pm$ 0.36 <sup>a</sup>	-0.47 $\pm$ 0.12 <sup>a</sup>	3.46 $\pm$ 0.17 <sup>a</sup>	74.61 $\pm$ 2.83 <sup>a</sup>
LGb	96.44 $\pm$ 0.60 <sup>a</sup>	-0.39 $\pm$ 0.17 <sup>a</sup>	3.05 $\pm$ 0.37 <sup>a</sup>	74.16 $\pm$ 8.16 <sup>a</sup>
LGc	96.39 $\pm$ 0.50 <sup>a</sup>	-0.43 $\pm$ 0.13 <sup>a</sup>	3.23 $\pm$ 0.26 <sup>a</sup>	74.77 $\pm$ 2.71 <sup>a</sup>

% HR. However, for EWP films produced by casting, the  $L$  and  $b^*$  values were lower than those observed in this study (Deng et al. 2022; Wu et al., 2023). The transmittance did not change significantly ( $p > 0.05$ ) for the different EWP films obtained, ranging values between 74.16 and 79.28 %. These values are very close to 80 %, the reference transmittance value to consider a material transparent (Guzmán-Puyol et al., 2022) and were similar to those obtained by Lee et al. (2013) for similar materials. The transmittance values were close to those obtained by Liu et al. (2023) for EWP films (79.83 %) and lower to the ones obtained by Lee et al. (2013) and Pranata et al. (2019) for similar films (89.4 % and 94.9 %, respectively). As explained by Pranata et al. (2019), this could be attributed to the higher orientation of the polymer chains obtained in an extrusion and calendering processing method compared to a compression-moulding processing.

### 3.3.5. Barrier properties of EWP films

The OP values of the EWP films ranged from  $4.28 \pm 0.82 \times 10^{-18}$  and  $1.68 \pm 0.18 \times 10^{-18} \text{ kg}\cdot\text{m}\cdot\text{m}^{-2}\cdot\text{s}^{-1}\cdot\text{Pa}^{-1}$  while the WVP values ranged from  $7.40 \pm 1.09 \times 10^{-13}$  to  $3.03 \pm 0.09 \times 10^{-13} \text{ kg}\cdot\text{m}\cdot\text{m}^{-2}\cdot\text{s}^{-1}\cdot\text{Pa}^{-1}$  (Fig. 7). These values were similar to those reported by Pranata et al. (2019) for EWP films ( $2.39 \pm 0.08 \times 10^{-18} \text{ kg}\cdot\text{m}\cdot\text{m}^{-2}\cdot\text{s}^{-1}\cdot\text{Pa}^{-1}$  and  $4.60 \pm 0.50 \times 10^{-13} \text{ kg}\cdot\text{m}\cdot\text{m}^{-2}\cdot\text{s}^{-1}\cdot\text{Pa}^{-1}$  for oxygen and water vapour, respectively) measured at similar conditions, although in this case the films were produced through extrusion and calendering. OP and WVP of the EWP films increased significantly ( $p < 0.001$  and  $p < 0.01$ , respectively) with increasing plasticiser proportions in the FFS formulations (Fig. 6). A similar phenomenon was observed in

other protein-based films, such as  $\beta$ -lactoglobulin films, where an increase in plasticiser content lead to a proportional increase in OP, indicating a linear relationship between the two variables (Sothornvit and Krochta, 2000). The observed increase in WVP values with an increasing plasticiser content has been previously reported by other authors in studies on protein-based films, such as whey protein isolate films (García-Anaya et al., 2025; Kokoszka et al., 2010; Osuna et al., 2022), and gelatine films (Ahmad et al., 2023). This phenomenon may be attributed to a reorganization of the protein network, driven by the ability of plasticisers to reduce protein-protein interactions by competing for hydrogen bonds and electrostatic interactions with the protein chains, which increases intermolecular spacing (García-Anaya et al., 2025; Krochta, 2002). Furthermore, a synergistic effect exists between glycerol and water. Water, acting as a plasticiser, not only reduces protein-protein interactions but also enhances polymer chain mobility and increases the film's free volume, thereby promoting moisture diffusion (Kokoszka et al., 2010). The glycerol/water ratio affects the properties of the resulting dough (Díazñez et al., 2020), with higher values observed for maximum torque and specific mechanical energy in mixtures with equal amounts of water and glycerol.

However, when comparing the three EWP grades studied for equal protein-to-plasticisers ratios, no significant differences in OP and WVP were observed, suggesting that the high temperature (130 °C) and pressure (2.9 MPa) applied during compression moulding may play a role in the reorganization of the proteins, obtaining films with similar gas transmission rates.

## 4. Conclusions

The gelling power of powdered egg white proteins is improved using different methods, such as dry heating, which induces structural changes that add to those produced during the spray-drying process. In the powdered egg white proteins with varying gelling capacities ( $5.13 \pm 0.29 \text{ N}$  in LG,  $10.00 \pm 1.88 \text{ N}$  in HG, and  $11.82 \pm 1.66 \text{ N}$  in EG) selected for this study, these changes were evident in different aspects. A positive correlation was observed between the gelling capacity and the  $\beta$ -sheet content in the secondary structure of the proteins. Moreover, EWP with the lowest gelling capacity exhibited the lowest content of soluble proteins.

The gelling capacity of powdered EWP will aid in selecting the appropriate protein-to-plasticiser ratio to ensure the viability of the film-forming solutions. Proteins that form hard gels, which are challenging to

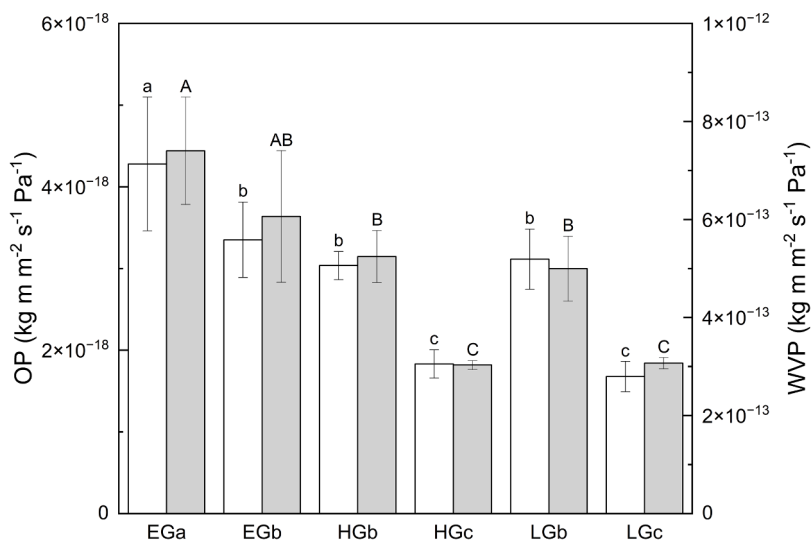


**Fig. 7.** Oxygen permeability (OP, white) and water vapour permeability (WVP, grey) of films developed with different EWP and protein/plasticiser ratios. Data are presented as mean values, and error bars indicate standard deviation ( $n = 6$ ). Significant differences ( $p < 0.05$ ) between films are presented with different letters: lower case letters refer for OP and capital letters for WVP.

process, require a protein-to-glycerol ratio below 2. To maintain the stability of the film-forming solutions, EWP with lower gelling capacity must be formulated with a protein-to-glycerol ratio greater than 1. As the gelling capacity of the proteins increased, the resulting FFS became more viscous, exhibiting higher consistency values and a lower flow index. The protein-to-plasticiser ratio also influenced the rheological behaviour of the FFS, as viscosity, storage modulus, and loss modulus decreased with increasing plasticiser content.

However, the properties of the films obtained via compression moulding depended more on the protein-to-plasticiser ratio than on the gelling capacity of the proteins used. Although the presence of protein clusters in some samples, as visualized by SEM, limited the evaluation of mechanical properties for all films, partial results indicated that the  $\beta$ -turn content in the secondary structure of the EWP and the plasticiser percentage are related with the tensile strength and Young's modulus ( $p < 0.05$ ), while  $\beta$ -turn content in the secondary structure of the EWP films is related to Young's modulus ( $p < 0.01$ ). All the films produced showed similar values in colour and transmittance, indicating that neither the gelling capacity of the EWP nor the plasticiser percentage influenced these parameters. As the plasticiser percentage increased in the FFS, the resulting films showed higher oxygen and water vapour permeability. This was expected, as the reduction in intermolecular forces between protein chains likely led to a polymer matrix with larger free volume or void spaces. However, films with the same protein-to-plasticiser ratio exhibited similar permeability values, regardless of the protein used.

Based on the obtained results, it can be concluded that the gelling capacity of EWP has not significant impact on the optical or barrier properties of films produced by compression moulding technology. However, the structural changes induced by the dry heating of EWP powder, reflected in the proteins' secondary structure, have been associated with certain of the mechanical properties of the films. Extrapolation of these results to other film manufacturing technologies, such as casting or injection moulding, should be done with caution, as should extrapolation to films produced with other proteins. This is because the structure of the polymer matrix is highly complex and may be influenced by other factors not addressed in this study.

#### Ethical statement - studies in humans and animals

The authors declare that this article does not contain any studies involving animals.

The authors declare that this article does not contain any studies involving humans.

#### CRediT authorship contribution statement

**Víctor Baquero-Aznar:** Writing – review & editing, Writing – original draft, Visualization, Investigation. **María L. Salvador:** Writing – review & editing, Visualization, Supervision, Resources, Methodology, Conceptualization. **Ángel Fernández-Cuello:** Writing – review & editing, Resources, Methodology. **Isabel Clavería:** Writing – review & editing, Resources, Methodology. **Jaime González-Buesa:** Writing – review & editing, Supervision, Resources, Methodology, Investigation, Funding acquisition, Conceptualization.

#### Declaration of competing interest

The authors declare that they have no known competing financial interests or personal relationships that could have appeared to influence the work reported in this paper.

#### Acknowledgements

This work was supported by the Ministerio de Ciencia e Innovación of Spain (projects PID2022–142850OR-I00 and PID2019–10808ORR-100, and pre-doctoral grant PRE2020–094379 to Víctor Baquero-

Aznar). It has also been supported by the Department of Industry and Innovation (Government of Aragon) through the research group Grant T07–23R. We would like to thank Jan Zijderveld from Bouwhuis Enthoven B. V. (Netherlands) for providing the different EWP commercial grades. Proteomic analyses were performed in the Proteomics Platform of Servicios Científico Técnicos del CIBA (IACS-Universidad de Zaragoza), ProteoRed ISCIII member. Authors acknowledge the use of instrumentation as well as the technical advice provided by the National Facility ELECOMI ICTS, node «Laboratorio de Microscopías Avanzadas (LMA)» at «Universidad de Zaragoza», particularly for the X-ray diffraction (XRD) and scanning electron microscopy (SEM) analyses.

#### Supplementary materials

Supplementary material associated with this article can be found, in the online version, at [doi:10.1016/j.fufo.2025.100616](https://doi.org/10.1016/j.fufo.2025.100616).

#### Data availability

Data will be made available on request.

#### References

- Ahmad, M.S., Ali, R.R., Majid, R.A., Mohamad, Z., 2023. Properties enhancement of packaging materials based on gelatin. *Environ. Qual. Manag.* 33 (2), 277–284. <https://doi.org/10.1002/tqem.21930>.
- ASTM, 2017. Standard Test Method For Oxygen Gas Transmission Rate Through Plastic Film and Sheeting Using a Coulometric Sensor. American Society for Testing Materials, Philadelphia. <https://doi.org/10.1520/D3985-17>. Method D3985-17.
- ASTM, 2018. Standard Test Method For Tensile Properties of Thin Plastic Sheeting. American Society for Testing Materials, Philadelphia. <https://doi.org/10.1520/D0882-18>. Method D882-18.
- ASTM, 2020. Standard Test Method For Water Vapor Transmission Rate Through Plastic Film and Sheeting Using a Modulated Infrared Sensor. American Society for Testing Materials, Philadelphia. <https://doi.org/10.1520/F1249-20>. Method F1249-20.
- Baquero, V., Salvador, M.L., González-Buesa, J., 2024. Effect of shellac coating on the properties of egg white protein (EWP) films for cherry tomato packaging. *Acta Horti* 1396, 375–384. <https://doi.org/10.17660/ActaHortic.2024.1396.50>.
- Barth, A., 2007. Infrared spectroscopy of proteins. *Biochim. Biophys. Acta* 1767 (9), 1073–1101. <https://doi.org/10.1016/j.bbabi.2007.06.004>.
- Bhaskar, R., Zo, S.M., Narayanan, K.B., Purohit, S.D., Gupta, M.K., Han, S.S., 2023. Recent development of protein-based biopolymers in food packaging applications: a review. *Polym. Test.* 124, 108097. <https://doi.org/10.1016/j.polymertesting.2023.108097>.
- Calva-Estrada, S.J., Jiménez-Fernández, M., Lugo-Cervantes, E., 2019. Protein-based films: advances in the development of biomaterials applicable to food packaging. *Food Eng. Rev.* 11, 78–92. <https://doi.org/10.1007/s12393-019-09189-w>.
- Chen, C.-H., Kuo, W.-S., Lai, L.-S., 2009. Rheological and physical characterization of film-forming solutions and ediblefilms from tapioca starch/decolorized hsian-tsoo leaf gum. *Food Hydrocoll* 23, 2132–2140. <https://doi.org/10.1016/j.foodhyd.2009.05.015>.
- Cheng, Y., Wang, J., Chi, Y., Ma, Z., Geng, X., Chi, Y., 2021. Effect of dry heating on egg white powder influencing water mobility and intermolecular interactions of its gels. *J. Sci. Food Agric.* 101, 433–440. <https://doi.org/10.1002/jsfa.10652>.
- Deng, W., Xu, Q., Hu, X., Sheng, L., 2022. Structure and properties of egg white protein films modified by high-intensity ultrasound: an effective strategy. *Food Res. Int.* 157, 111264. <https://doi.org/10.1016/j.foodres.2022.111264>.
- Deseta, M.L., Sponton, O.E., Finos, M.B., Cuffia, F., Torres-Nicolini, A., Álvarez, V.A., Santiago, L.G., Pérez, A.A., 2023. Development of antifungal films from nanocomplexes based on egg white protein nanogels and phenolic compounds. *Food Biophys* 18 (2), 273–288. <https://doi.org/10.1007/s11483-022-09770-7>.
- Díaz, I., Martínez, I., Gómez, P.A., 2020. Effect of plasticiser on the morphology, mechanical properties and permeability of albumen-based nanobiocomposites. *Food Packag. Shelf Life* 24, 100499. <https://doi.org/10.1016/j.fpsl.2020.100499>.
- Dong, M., Tian, L., Li, J., Jia, J., Dong, Y., Tu, Y., Liu, X., Tan, C., Duan, X., 2022. Improving physicochemical properties of edible wheat gluten protein films with proteins, polysaccharides and organic acid. *LTW* 154, 112868. <https://doi.org/10.1016/j.lwt.2021.112868>.
- Dong, X., Zhang, Y.-Q., 2020. An insight on egg white: from most common functional food to biomaterial application. *J. Biomed. Mater. Res.* 109, 1045–1058. <https://doi.org/10.1002/jbm.b.34768>.
- Félix, M., Martín-Alfonso, J.E., Romero, A., Guerrero, A., 2014. Development of albumen/soy biobased plastic materials processed by injection molding. *J. Food Eng.* 125 (1), 7–16. <https://doi.org/10.1016/j.jfoodeng.2013.10.018>.
- Félix, M., Pérez-Puyana, V., Romero, A., Guerrero, A., 2017. Development of protein-based bioplastics modified with different additives. *J. Appl. Polym. Sci.* 134, 45430. <https://doi.org/10.1002/app.45430>.
- Fernández-Espada, L., Bengoechea, C., Cordobés, F., Guerrero, A., 2013. Linear viscoelasticity characterization of egg albumen/glycerol blends with applications in

- material moulding processes. *Food Bioprod. Process.* 91 (4), 319–326. <https://doi.org/10.1016/j.fbp.2012.11.009>.
- García-Anaya, M., Sepúlveda, D.R., Zamudio-Flores, P.B., Acosta-Muñiz, C.H., 2025. Effect of the glycerol content on the A511 bacteriophage release in films made with whey protein isolated. *J. Food Eng.* 388, 112388. <https://doi.org/10.1016/j.jfoodeng.2024.112388>.
- Ghasemlou, M., Barrow, C.J., Adhikari, B., 2024. The future of bioplastics in food packaging: an industrial perspective. *Food Packag. Shelf Life* 43, 101279. <https://doi.org/10.1016/j.fpsl.2024.101279>.
- González-Gutiérrez, J., Partal, P., García-Morales, M., Gallegos, C., 2010. Development of highly-transparent protein/starch-based bioplastics. *Bioresour. Technol.* 101 (6), 2007–2013. <https://doi.org/10.1016/j.biortech.2009.10.025>.
- González-Gutiérrez, J., Partal, P., García-Morales, M., Gallegos, C., 2011. Effect of processing on the viscoelastic, tensile and optical properties of albumen/starch-based bioplastics. *Carbohydr. Polym.* 84 (1), 308–315. <https://doi.org/10.1016/j.carbpol.2010.11.040>.
- Guzman-Puyol, S., Benítez, J.J., Heredia-Guerrero, J.A., 2022. Transparency of polymeric food packaging materials. *Food Res. Int.* 161, 111792. <https://doi.org/10.1016/j.foodres.2022.111792>.
- Han, K., Liu, Y., Liu, Y., Huang, X., Sheng, L., 2020. Characterization and film-forming mechanism of egg white/pullulan blend film. *Food Chem* 315, 126201. <https://doi.org/10.1016/j.foodchem.2020.126201>.
- Hernández-Izquierdo, V.M., Krochta, J.M., 2008. Thermoplastic processing of proteins for film formation - a review. *J. Food Sci.* 73 (2), R30–R39. <https://doi.org/10.1111/j.1750-3841.2007.00636.x>.
- Huang, X., Luo, X., Liu, L., Dong, K., Yang, R., Lin, C., Song, H., Li, S., Huang, Q., 2020. Formation mechanism of egg white protein/κ-carrageenan composite film and its application to oil packaging. *Food Hydrocoll* 105, 105780. <https://doi.org/10.1016/j.foodhyd.2020.105780>.
- Ishihama, Y., Oda, Y., Tabata, T., Sato, T., Nagasu, T., Rappsilber, J., Mann, M., 2005. Exponentially modified protein abundance index (emPAI) for estimation of absolute protein amount in proteomics by the number of sequenced peptides per protein. *Mol. Cell. Proteomics* 4 (9), 1265–1272. <https://doi.org/10.1074/mcp.M500061-MCP200>.
- Jerez, A., Partal, P., Martínez, I., Gallegos, C., Guerrero, A., 2007. Egg white-based bioplastics developed by thermomechanical processing. *J. Food Eng.* 82 (4), 608–617. <https://doi.org/10.1016/j.jfoodeng.2007.03.020>.
- Jiang, S., Zhang, J., Zhang, M., Qian, F., Mu, G., 2024. Characteristics of whey protein concentrate/egg white protein composite film modified by transglutaminase and its application on cherry tomatoes. *J. Food Sci.* 89, 9529–9542. <https://doi.org/10.1111/1750-3841.17506>.
- Jones, A., Zeller, M.A., Sharma, S., 2013. Thermal, mechanical, and moisture absorption properties of egg white protein bioplastics with natural rubber and glycerol. *Prog. Biomater.* 2, 12. <https://doi.org/10.1186/2194-0517-2-12>.
- Kang, H., Wang, Z., Zhang, W., Li, J., Zhang, S., 2016. Physico-chemical properties improvement of soy protein isolate films through caffeic acid incorporation and tri-functional aziridine hybridization. *Food Hydrocoll* 61, 923–932. <https://doi.org/10.1016/j.foodhyd.2016.07.009>.
- Katekhong, W., Charoenrein, S., 2018. Influence of spray drying temperatures and storage conditions on physical and functional properties of dried egg white. *Dry. Technol.* 36 (2), 169–177. <https://doi.org/10.1080/07373937.2017.1307218>.
- Kokoszka, S., Debeaufort, F., Lenart, A., Voilley, A., 2010. Water vapour permeability, thermal and wetting properties of whey protein isolate based edible films. *Int. Dairy J.* 20 (1), 53–60. <https://doi.org/10.1016/j.idairyj.2009.07.008>.
- Koyama, S., Nemoto, Y., Ichikawa, M., Oka, D., Tsujii, Y., Noguchi, T., Tokano, K., Handa, A., 2021. Effects of suppressing protein structural changes on the excellent gelling properties of dried egg white via dry-heat treatment. *Food Sci. Technol. Res.* 27 (2), 293–300. <https://doi.org/10.3136/fstr.27.293>.
- Koyama, S., Kodama, D., Tsujii, Y., Handa, A., 2023. Soluble-protein-aggregate-assisted improvements in heat-induced gel properties: effect of genipin-mediated crosslinks on egg white protein. *LWT* 184, 115079. <https://doi.org/10.1016/j.lwt.2023.115079>.
- Koyama, S., Kodama, D., Handa, A., Tsujii, Y., 2024. Dry-heat-induced phosphoserine-specific fragmentation of ovalbumin. *Food Chem* 440, 138263. <https://doi.org/10.1016/j.foodchem.2023.138263>.
- Krochta, J.M., 2002. Proteins as raw materials for films and coatings: definitions, current status, and opportunities. In: Gennadios, A. (Ed.), *Protein-Based Films and Coatings*, 1st Edition. CRC Press, New York, pp. 1–41.
- Kumar, L., Ramakanth, D., Akhila, K., Gaikwad, K.K., 2021. Edible films and coatings for food packaging applications: a review. *Environ. Chem. Lett.* 20 (1), 875–900. <https://doi.org/10.1007/s10311-021-01339-z>.
- Lechevalier, V., Guérin-Dubiard, C., Anton, M., Beaumont, V., Briand, E.D., Gillard, A., Le Gouar, Y., Musikhaphun, N., Pasco, M., Dupont, D., Nau, F., 2017. Effect of dry heat treatment of egg white powder on its functional, nutritional and allergenic properties. *J. Food Eng.* 195, 40–51. <https://doi.org/10.1016/j.jfoodeng.2016.09.022>.
- Lee, R.S., Pranata, M., Ustunol, Z., Almenar, E., 2013. Influence of glycerol and water activity on the properties of compressed egg white-based bioplastics. *J. Food Eng.* 118 (1), 132–140. <https://doi.org/10.1016/j.jfoodeng.2013.03.031>.
- Li, C., Li, F., Wang, K., Zhao, Y., Xie, D., 2024. Antimicrobial packaging film with finger wrinkles structures based on egg white and chitosan coating for fruit preservation. *Int. J. Biol. Macromol.* 283, 137888. <https://doi.org/10.1016/j.ijbiomac.2024.137888>.
- Li, P., Jin, Y., Sheng, L., 2020. Impact of microwave assisted phosphorylation on the physicochemical and rehydration behaviour of egg white powder. *Food Hydrocoll* 100, 105380. <https://doi.org/10.1016/j.foodhyd.2019.105380>.
- Li, X., Lv, J., Niu, M., Liu, S., Wu, Y., Liu, J., Xie, J., Sun, C., Wang, Y.-M., 2023. Characterization and antibacterial properties of egg white protein films loaded with “polylysine: evaluation of their degradability and application. *Foods* 12, 2431. <https://doi.org/10.3390/foods1222431>.
- Li-Chan, E.C.Y., Powrie, W.D., Nakai, S., 2007. *The chemistry of eggs and egg products*. In: Stadelman, W.J., Cotterill, O.J. (Eds.), *Egg Science and Technology* (Fourth). Haworth Press, Binghamton, New York, pp. 105–176.
- Liu, J., Wang, Y., Lv, J., Wu, Y., Guo, Y., Sun, C., Li, X., 2023. Biodegradable composite films based on egg white protein and tea polyphenol: physicochemical, structural and antibacterial properties. *Food Packag. Shelf Life* 38, 101098. <https://doi.org/10.1016/j.fpsl.2023.101098>.
- Liu, L., Huang, X., Geng, F., Huang, Q., 2022. Optimization of preparation process of egg white protein/κ-carrageenan composite film. *J. Food. Process. Preserv.* 46, e16167. <https://doi.org/10.1111/jfpp.16167>.
- Liu, S., Qiao, S., Zhu, J., Yang, Y., Chen, H., Dai, H., Zhu, H., Yu, Y., Ma, L., Zhang, Y., Wang, H., 2024. Enhanced barrier and antioxidant properties of gelatin films by structural-colored bioactive materials for food packaging. *Food Hydrocoll* 150, 109744. <https://doi.org/10.1016/j.foodhyd.2024.109744>.
- López-Castejón, M.L., Bengoechea, C., García-Morales, M., Martínez, I., 2015. Effect of plasticizer and storage conditions on thermomechanical properties of albumen/tragacanth based bioplastics. *Food Bioprod. Process.* 95, 264–271. <https://doi.org/10.1016/j.fbp.2014.11.002>.
- López-Castejón, M.L., Bengoechea, C., García-Morales, M., Martínez, I., 2016. Influence of tragacanth gum in egg white based bioplastics: thermomechanical and water uptake properties. *Carbohydr. Polym.* 152, 62–69. <https://doi.org/10.1016/j.carbpol.2016.06.041>.
- López-Mata, M.A., García-González, G., Valbuena-Gregorio, E., Ruiz-Cruz, S., Zumudio-Flores, P.B., Burrull-Ibarra, S.E., Morales-Figueroa, G.G., Quihui-Cota, L., 2016. Development and characteristics of biodegradable aloe-gel/egg white films. *J. Appl. Polym. Sci.* 44067. <https://doi.org/10.1002/APP.44067>.
- Ma, Y., Zhao, Y., Chi, Y., 2019. Changes in the gel characteristics of two hen egg white powders modified by dry heating and the Maillard reaction during long-term storage. *LWT* 109, 123–129. <https://doi.org/10.1016/j.lwt.2019.04.003>.
- Ma, Y., Shan, A., Wang, R., Zhao, Y., Chi, Y., 2021. Characterization of egg white powder gel structure and its relationship with gel properties influenced by pretreatment with dry heat. *Food Hydrocoll* 110, 106149. <https://doi.org/10.1016/j.foodhyd.2020.106149>.
- Ma, Y., Qing, M., Zang, J., Shan, A., Zhang, H., Chi, Y., Chi, Y., Gao, X., 2022. Molecular interactions in the dry heat-facilitated hydrothermal gel formation of egg white protein. *Food Res. Int.* 162, 112058. <https://doi.org/10.1016/j.foodres.2022.112058>.
- Mihalca, V., Kerezsi, A.D., Weber, A., Gruber-Traub, C., Schmucker, J., Vodnar, D.C., Dulif, F.V., Socaci, S.A., Fărcaș, A., Mureșan, C.I., Suharoschi, R., Pop, O.L., 2021. Protein-based films and coatings for food industry applications. *Polymers (Basel)* 13 (5), 769. <https://doi.org/10.3390/polym13050769>.
- Niegelhell, K., Süßenbacher, M., Sattelkow, J., Plank, H., Wang, Y., Zhang, K., Spirk, S., 2017. How bound and free fatty acids in cellulose films impact nonspecific protein adsorption. *Biomacromolecules* 18 (12), 4224–4231. <https://doi.org/10.1021/acs.biomac.7b01260>.
- Ogale, A.A., Cunningham, P., Dawson, P.L., Acton, J.C., 2000. Viscoelastic, thermal, and microstructural characterization of soy protein isolate films. *J. Food Sci.* 65 (4), 672–679. <https://doi.org/10.1111/j.1365-2621.2000.tb16071.x>.
- Osuna, M.B., Michaluk, A., Romero, A.M., Judis, M.A., Bertola, N.C., 2022. Plasticizing effect of *Apis mellifera* honey on whey protein isolate films. *Biopolymers* 113 (8), e23519. <https://doi.org/10.1002/bip.23519>.
- Peng, N., Gu, L., Li, J., Chang, C., Li, X., Su, Y., Yang, Y., 2017. Films based on egg white protein and succinylated casein cross-linked with transglutaminase. *Food Bioprocess Technol* 100, 1422–1430. <https://doi.org/10.1007/s11947-017-1901-8>.
- Peña-Cháidez, J.E., Rosas-Flores, W., Salazar-Montoya, J.A., Morales-Contreras, B.E., Gallegos-Infante, J.A., Morales-Castro, J., Medrano-Roldán, H., 2021. Rheological and thermal characterization of pinto saltillo bean (*Phaseolus vulgaris* L.) protein isolates/sodium alginate gels. *LWT* 146, 111419. <https://doi.org/10.1016/j.lwt.2021.111419>.
- Plastics Europe, 2023. *Plastics - the fast facts 2023*. <https://plasticseurope.org/es/plastics-europe-publica-plastics-the-fast-facts-2023/> (accessed 12 March 2025).
- Pranata, M.P., González-Buesa, J., Chopra, S., Kim, K., Pietri, Y., Ng, P.K.W., Matuana, L.M., Almenar, E., 2019. Egg white protein film production through extrusion and calendaring processes and its suitability for food packaging applications. *Food Bioprocess Technol* 12 (4), 714–727. <https://doi.org/10.1007/s11947-019-2248-0>.
- Proaño, J.L., Salgado, P.R., Cian, R.E., Mauri, A.N., Drago, S.R., 2020. Physical, structural and antioxidant properties of brewer's spent grain protein films. *J. Sci. Food Agric.* 100 (15), 5458–5465. <https://doi.org/10.1002/jsfa.10597>.
- Qin, X., Cai, X., Wang, Y., Chen, L., Zhao, J., Zhang, Y., Bi, S., Zhou, Y., Zhu, Q., Cheng, Y., Liu, Y., 2024. A water-resistant egg white/chitosan/pectin blending film with spherical-linear molecular interpenetrating network strengthened by multifunctional tannin-nisin nanoparticles. *Int. J. Biol. Macromol.* 277, 134548. <https://doi.org/10.1016/j.ijbiomac.2024.134548>.
- Razi, S.M., Fahim, H., Amirabadi, S., Rashidinejad, A., 2023. An overview of the functional properties of egg white proteins and their application in the food industry. *Food Hydrocoll* 135, 108183. <https://doi.org/10.1016/j.foodhyd.2022.108183>.
- Rojas-Lema, S., Nilsson, K., Langton, M., Trifol, J., Gomez-Caturla, J., Balart, R., García-García, D., Moriana, R., 2023. The effect of pine cone lignin on mechanical, thermal and barrier properties of faba bean protein films for packaging applications. *J. Food Eng.* 339, 111282. <https://doi.org/10.1016/j.jfoodeng.2022.111282>.

- Rouilly, A., Mériaux, A., Geneau, C., Silvestre, F., Rigal, L., 2006. Film extrusion of sunflower protein isolate. *Polym. Eng. Sci.* 46 (11), 1635–1640. <https://doi.org/10.1002/pen.20634>.
- Shin, M., Han, Y., Ahn, K., 2013. The influence of the time and temperature of heat treatment on the allergenicity of egg white proteins. *Allergy Asthma Immunol. Res.* 5 (2), 96–101. <https://doi.org/10.4168/aaair.2013.5.2.96>.
- Sobral, P.J.A., dos Santos, J., Garcia, F.T., 2005. Effect of protein and plasticizer concentrations in film forming solutions on physical properties of edible films based on muscle proteins of a Thai Tilapia. *J. Food Eng.* 70, 93–100. <https://doi.org/10.1016/j.jfoodeng.2004.09.015>.
- Sothornvit, R., Krochta, J.M., 2000. Plasticizer effect on oxygen permeability of  $\beta$ -lactoglobulin films. *J. Agric. Food Chem.* 48 (12), 6298–6302. <https://doi.org/10.1021/jf000836l>.
- Strixner, T., Kulozik, U., 2011. Egg proteins. In: Phillips, G.O., Williams, P.A. (Eds.), *Handbook of Food Proteins*. Woodhead Publishing, Sawston, pp. 150–209. <https://doi.org/10.1533/9780857093639.150>. ISBN: 978-1-84569-758-7.
- Su, Y., Dong, Y., Niu, F., Wang, C., Liu, Y., Yang, Y., 2015. Study on the gel properties and secondary structure of soybean protein isolate/egg white composite gels. *Eur. Food Res. Technol.* 240 (2), 367–378. <https://doi.org/10.1007/s00217-014-2336-3>.
- Sun, H., Huang, Y., Chen, Y., Liu, X., Leng, X., 2023. Effects of curcumin, phycoyanin, or modified lycopene colorants on the physicochemical and sensory properties of whey protein–cellulose nanocrystal packaging films. *Food Chem* 412, 135541. <https://doi.org/10.1016/j.foodchem.2023.135541>.
- Sun, J., Liu, T., Zhang, F., Huang, Y., Zhang, Y., Xu, B., 2022. Tea polyphenols on emulsifying and antioxidant properties of egg white protein at acidic and neutral pH conditions. *LWT* 153, 112537. <https://doi.org/10.1016/j.lwt.2021.112537>.
- Sun, Y., Liu, Z., Zhang, L., Wang, X., Li, L., 2020. Effects of plasticizer type and concentration on rheological, physico-mechanical and structural properties of chitosan/zein film. *Int. J. Biol. Macromol.* 143, 334–340. <https://doi.org/10.1016/j.ijbiomac.2019.12.035>.
- Susi, H., Byler, D.M., 1983. Protein structure by fourier transform infrared spectroscopy: second derivative spectra. *Biochem. Biophys. Res. Commun.* 115 (1), 391–397. [https://doi.org/10.1016/0006-291X\(83\)91016-1](https://doi.org/10.1016/0006-291X(83)91016-1).
- Tian, X., Lian, S., Wen, J., Chen, Z., Wang, S., Hu, J., Peng, H., Peng, Y., 2018. Egg albumin-assisted sol-gel synthesis and photo-catalytic activity of SnO<sub>2</sub> micro/nano-structured biscuits. *J. Sol-Gel Sci. Technol.* 85 (2), 402–412. <https://doi.org/10.1007/s10971-017-4547-0>.
- Verbeek, C.J.R., van den Berg, L.E., 2010. Extrusion processing and properties of protein-based thermoplastics. *Macromol. Mater. Eng.* 295 (1), 10–21. <https://doi.org/10.1002/mame.200900167>.
- Wang, J., Peng, P., Li, J., Chen, Y., Lv, Y., Meng, X., 2025. Functional modification of edible film based on egg white protein and its application in food preservation: a review. *Int. J. Biol. Macromol.* <https://doi.org/10.1016/j.ijbiomac.2025.142096>.
- Wei, W., Hu, W., Zhang, X.-Y., Zhang, F.-P., Sun, S.-Q., Liu, Y., Xu, C.-H., 2018. Analysis of protein structure changes and quality regulation of surimi during gelation based on infrared spectroscopy and microscopic imaging. *Sci. Rep.* 8 (1), 5566. <https://doi.org/10.1038/s41598-018-23645-3>.
- Weng, S., Marcet, I., Rendueles, M., Díaz, M., 2024. Edible films from the laboratory to industry: a review of the different production methods. *Food Bioprocess Technol.* <https://doi.org/10.1007/s11947-024-03641-4>.
- Wu, Y., Wang, Y., Lv, J., Jiao, H., Liu, J., Feng, W., 2023. Preparation and characterization of egg white protein film incorporated with epigallocatechin gallate and its application on pork preservation. *Food Chem. X* 19, 100791. <https://doi.org/10.1016/j.fochx.2023.100791>.
- Wu, Y., Wu, H., Hu, L., 2024. Recent advances of proteins, polysaccharides and lipids-based edible films/coatings for food packaging applications: a review. *Food Biophys* 19 (1), 29–45. <https://doi.org/10.1007/s11483-023-09794-7>.
- Xiao, Y., Xu, H., Zhou, Q., Li, W., Gao, J., Liao, X., Yu, Z., Zheng, M., Zhou, Y., Sui, X., Liu, Y., 2023. Influence mechanism of wheat bran cellulose and cellulose nanocrystals on the storage stability of soy protein isolate films: conformation modification and molecular. *Food Hydrocoll.* 139, 108475. <https://doi.org/10.1016/j.foodhyd.2023.108475>.
- Yao, X., Ma, J., Lv, X., Liu, X., Chen, R., Shan, Y., Zeng, Q., 2024. Structural and functional optimization of egg white protein hydrogels by succinylation: gel properties and mineral enrichment. *Int. J. Biol. Macromol.* 282, 137585. <https://doi.org/10.1016/j.ijbiomac.2024.137585>.
- Yuno-Ohta, N., Saito, H., Onda, T., Handa, A., 2021. Characterization of the effect of dry-heat treatment on the gelation of alkaline dried egg whites using dynamic viscoelastic measurement and ultrasound spectroscopy. *Colloids Surf. B Biointerfaces* 208, 112051. <https://doi.org/10.1016/j.colsurfb.2021.112051>.
- Zhao, X., Mu, Y., Dong, H., Zhang, H., Zhang, H., Chi, Y., Song, G., Li, H., Wang, L., 2020. Effect of cinnamaldehyde incorporation on the structural and physical properties, functional activity of soy protein isolate-egg white composite edible films. *J. Food Process. Preserv.* 45, e15143. <https://doi.org/10.1111/jfpp.15143>.